Available online at www.sciencedirect.com

ScienceDirect

journal homepage: www.elsevier.com/locate/he

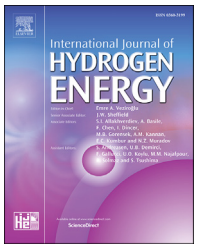

Characterization of Powder River Basin coal pyrolysis with cost-effective and environmentally-friendly composite Na–Fe catalysts in a thermogravimetric analyzer and a fixed-bed reactor

Bang Xu [a], *Dongyang Kuang* [b], *Fangjing Liu* [a], *Wenyang Lu* [a], *Alexander K. Goroncy* [c], *Ting He* [d], *Khaled Gasem* [a], *Maohong Fan* [a,e,*]

[a] *Departments of Chemical Engineering & Petroleum Engineering, University of Wyoming, Laramie, WY 82071, USA*
[b] *Department of Mathematics, Southern Utah University, Cedar City, UT 84720, USA*
[c] *Department of Chemistry, University of Wyoming, Laramie, WY 82071, USA*
[d] *Idaho National Laboratory, Idaho Falls, ID 83415, USA*
[e] *School of Energy Resources, University of Wyoming, Laramie, WY 82071, USA*

ARTICLE INFO

Article history:
Received 24 October 2017
Received in revised form
8 January 2018
Accepted 15 February 2018
Available online 12 March 2018

Keywords:
Catalytic pyrolysis
Coal
Na–Fe catalyst
Kinetics analysis
Catalytic mechanism

ABSTRACT

The pyrolysis characteristics of PRB coal with use of Na–Fe composite catalysts were investigated in a thermogravimetric analyzer and a fixed bed reactor. Model-free methods developed by Friedman (FR), Kissinger-Akahira-Sunose (KAS), Flynn-Wall-Ozawa (FWO) and Vyazovkin (VA) were compared and applied to determine the pyrolysis kinetic parameters. A Master-plot method was used to determine the reaction order and pre-exponential factors. Raw coal with the addition of 4% $FeCO_3$ achieved the highest effect on coal conversion; specifically, 4% Na_2CO_3 and 1% Na_2CO_3–3% $FeCO_3$ showed higher effect than 3% Na_2CO_3–1% $FeCO_3$ and 2% Na_2CO_3–2% $FeCO_3$. The averaged E values of raw coal with 4% $FeCO_3$ catalyst decreased by 10% compared with that of raw coal. Compared with the individual use of 4% Na_2CO_3, the addition of $FeCO_3$ can be effective in decreasing the E values of the raw coal. The nonlinear VA method appears to be superior in determining activation energies of coal pyrolysis at considered conversion range. Further, the A_n (random nucleation and nuclei growth model) appears to be the appropriate reaction model for raw coal pyrolysis with and without the use of Na–Fe composite catalysts. From the pyrolysis in the fixed bed reactor, XRD and FTIR tests for coal chars produced by PRB coal pyrolysis with use of catalysts were conducted. By combining the gas evolution and XRD/FTIR results, a reaction mechanism is proposed for coal pyrolysis with composite Na_2CO_3–$FeCO_3$ catalysts.

* *Corresponding author*. Departments of Chemical Engineering & Petroleum Engineering, University of Wyoming, Laramie, WY 82071, USA.
E-mail address: mfan@uwyo.edu (M. Fan).
https://doi.org/10.1016/j.ijhydene.2018.02.102

Introduction

The rising interest in clean coal conversion and utilization technology is expanding research efforts in coal science and engineering worldwide. As a key step in coal thermochemical conversion technology, gasification and combustion processes, pyrolysis and its applications is a point of focus for such researches. By means of pyrolysis, coal can be converted into useful energy holder (bio-oil), adsorbent bio-char and various useful-chemicals such as benzene, toluene, naphthalene, phenol, creosote oil, and so on [1,2]. However, conventional coal pyrolysis techniques are often plagued with problems, such as low efficiency of coal conversion, high contents of oxygen and heavy component (boiling point higher than 360 °C) in the coal oil product, difficulties in separating coal particle and coal oil. Thus, coal catalytic pyrolysis has become exceedingly desirable technology to improve coal pyrolysis conversion and orientation of pyrolysis products, especially developing a cost-effective and environmentally-friendly catalyst.

Previously, catalysts used in the pyrolysis of coal mainly include alkali and alkaline earth metallic compounds, transition metallic compounds, natural minerals, or mineral matters in coal [3–6]. It has been demonstrated that alkali metal carbonates, such as Na_2CO_3 and K_2CO_3, can improve the gas yield and reduce tar and char yields during coal pyrolysis. Moreover, some results indicate that the addition of Na_2CO_3 can improve the quality of pyrolysis oil produced by oil sludge and biomass. Also, the oxygen content of the bio-oil from biomass pyrolysis is decreased from 47.5 wt.% to 16.4 wt.% with Na_2CO_3 [4,7,8]. These results suggest that Na_2CO_3 is a potentially superior catalyst for producing chemicals by coal pyrolysis and gasification. Meanwhile, iron-based catalysts are also widely used in coal pyrolysis and gasification due to its low price, favorable environmental attributes, and its better catalytic activity for hydrogenation reactions. Studies have shown that Fe_2CO_3 catalyst can be decomposed into iron oxides and then be reduced to iron and iron carbide above 719 °C during coal pyrolysis [9,10]. Fe_2CO_3 could help decompose most of the hydrocarbons at 900 °C, producing only a small amount of CH_4 [11], which is beneficial to coal-to-liquid utilization processes.

Proper use of composite catalysts has the potential to improve reaction rates and production rates of desirable products when compared with the use of individual catalysts. By using the composite Na_2CO_3–$FeCO_3$ catalysts, one may expect some advantages such as changes in the selectivity of H_2/CO and tar yields, increased conversion rate or general improvements of the overall efficiency of pyrolysis and gasification. With these aims, the knowledge of pyrolysis kinetics of coal with the use of composite Na_2CO_3–$FeCO_3$ catalysts deserves a careful study. This will be critical to the goal of developing new coal conversion technologies and to the design of proper and efficient reactors.

Thermogravimetric analysis (TGA) is one of the most common techniques used to investigate the characteristics of decomposition and kinetic parameters during pyrolysis of solid samples such as coal, biomass, plastic, and so on [12,13]. Historically, various methods were applied in evaluating devolatilization kinetic process of solid fuels using non-isothermal TG analysis, especially some popular model-free methods developed by Friedman (FR) [14], Flynn-Wall-Ozawa (FWO) [15,16], Kissinger-Akahira-Sunose (KAS) [17,18] and Vyazovkin (V) [19,20]. These methods are based on the assumption that the reaction rate at a constant extent of conversion only depends on the temperature. Hence, the activation energy can be evaluated without the need of a reaction model. Moreover, many methods including master plot methods, Popescu and Satave [21–23] methods have been developed to establish the kinetic model of thermal decomposition of solid fuels without assuming of kinetic model. All methods were adopted in this study to calculate kinetic parameters of coal pyrolysis with and without catalysts.

In our present work, Powder River Basin (PRB) coal has been analyzed by proximate analysis, ultimate analysis, FTIR analysis, X-ray diffraction analysis, and solid state ^{13}C NMR analysis to obtain its physical and chemical characteristics. In addition, the pyrolysis behavior of coal with and without composite Na_2CO_3–$FeCO_3$ catalysts were studied using a thermogravimetric analyzer and a fixed-bed reactor. The aim is to investigate effects of catalysts and heating rate on the pyrolysis process of coal and to study pyrolysis kinetic characteristics of coal with and without catalysts. The activation energies were estimated by model-free methods, which includes KAS, FWO, FR, and VA. In addition, From the pyrolysis in the fixed bed reactor, XRD and FTIR tests for coal chars produced by PRB coal pyrolysis with use of catalysts were conducted. The catalytic mechanism of PRB coal pyrolysis with Na_2CO_3–$FeCO_3$ composite catalysts was proposed.

Material and methods

Sample preparation

Raw coal used in this work is from the Wyoming Powder River Basin and is provided by Wyodak Resources Development Corp. The proximate analysis was measured according to ASTM D5142 and D5016 [24]. The ultimate analysis (C, H, N, and S) of raw coal was performed using the elemental analyzer (Vario EL cube, Germany) and the oxygen (O) content was calculated by difference. The results of proximate and ultimate analysis of the coal are shown in Table 1. The ash of raw coal was prepared by air oxidation at 1088K in a high temperature furnace and the chemical composition was determined by XRF-1800. These results are presented in Table 2.

The incipient wetness impregnation (IWI) method was used to mix $FeCO_3$ and Na_2CO_3 with the coal particles. The

Table 1 – Proximate and ultimate analyses and high heating value of raw coal.

Proximate analysis (wt.%)			Ultimate analysis (wt.%, daf)					HHV (MJ/kg)
M_{ad}	A_d	V_{daf}	C	H	N	S	O[a]	
10.27	8.72	48.73	78.87	3.72	1.01	0.47	15.93	29.57

[a] By difference.

Table 2 – Analysis of raw coal ash.

Element	(wt%)	Oxide	(wt%)
Si	14.24	SiO_2	31.77
Al	7.59	Al_2O_3	14.97
Fe	4.23	Fe_2O_3	6.31
Mg	3.83	MgO	6.62
Ca	18.73	CaO	27.33
Ti	0.6	TiO_2	1.04
K	0.66	K_2O	0.83
P	0.51	P_2O_5	1.22
Na	1.26	Na_2O	1.77
Mn	0.02	MnO_2	0.04
Ba	0.35	BaO	0.41
Sr	0.41	SrO	0.51
S	2.76	SO_3	7.19

specific preparation of the $FeCO_3$ catalyst has been described in detail elsewhere [9,25]. The catalyst and coal mixtures were prepared by adding the appropriate amounts of $FeCO_3$, Na_2CO_3, or $FeCO_3$–Na_2CO_3 to PRB pulverized coal to obtain the following weight ratios of catalyst to dry ash free (DAF) basis coal: 4% Na_2CO_3 (4% Na), 3% Na_2CO_3-1% $FeCO_3$ (3% Na–1% Fe), 2% Na_2CO_3-2% $FeCO_3$ (2% Na–2% Fe), 1% Na_2CO_3-3% $FeCO_3$(1% Na–3% Fe) and 4% $FeCO_3$ (4% Fe).

TG analysis

A SDT Q600 apparatus was employed for TGA experiments. For each experimental run, samples were heated at predetermined heating rates β = 10, 20, 30, 40, and 50 °C/min to a final pyrolysis temperature at 900°Cand held at that temperature for 10 min. Also, nitrogen was used as the purge gas at 100 ml/min. The mass of coal samples ranged from 5 to 10 mg and particle size less than 125 μm were used to lower the temperature gradient.

The weight loss rate was calculated by the following equation

$$\frac{dw}{dt} = -\frac{1}{w_0}\left(\frac{dw_t}{dt}\right) \quad \text{(E1)}$$

The reaction degree, x, was calculated by

$$x = \frac{w_0 w_t}{w_0 w_f} \quad \text{(E2)}$$

where w_t is the sample mass at given time t/temperature T, while w_0 and w_f are the masses of coal sample prior to and after the tests when the temperature was at 900 °C. During the calculation process, the mass loss of the catalysts was ignored during the pyrolysis.

Fixed-bed pyrolysis procedure

As described in our previous study [26], the pyrolysis test was conducted in a fixed-bed reactor system. For each experiment, a sample about 5.0 g DAF coal (smaller than 125 μm) was placed in the reactor, then was heated at 10 °C/min to the desired pyrolysis temperatures 900 °C in N_2 with a flow rate of 15 ml/min, followed by keeping the system at the same temperature for pyrolysis for 30 min. The uncondensed gas was passed through a desiccant-filled water trap for removing water, then analyzed by gas chromatograph, Agilent 3000A micro GC, equipped with two micro-columns, namely 18, MolSieve 5A PLOT and 4 PoraPlot U to separate H_2, CO, N_2, CO_2 and CH_4, prior to concentration analysis using thermal conductivity detector (TCD).

Kinetic theory

Activation energy

The decomposition or pyrolysis of coal is generally represented in the form of

$$A(s) \rightarrow B(g) + C(s) \quad \text{(R1)}$$

The kinetic model of R1 can be expressed following as [27].

$$\frac{d\alpha}{dt} = k(T)f(\alpha) = A\exp\left(-\frac{E}{RT}\right)f(\alpha) \quad \text{(E3)}$$

where t is time, α is pyrolysis reaction degree, $\alpha = \frac{w_0 - w_t}{w_0 - w_f}$, and $k(T)$ is temperature dependent rate constant, $f(\alpha)$ is reaction model, A is the pre-exponential Arrhenius factor (usually assumed to be independent of temperature), E is the activation energy, and R is universal gas constant.

Under non-isothermal condition, β = dT/dt (K/min), is a variable. E3 can be changed to

$$\beta\frac{d\alpha}{dT} = A\exp\left(-\frac{E}{RT}\right)f(\alpha) \quad \text{(E4)}$$

The integration of E4 gives [28].

$$\int_0^{\alpha}\frac{\delta\alpha}{\varphi(\alpha)} = g(\alpha) = \frac{A}{\beta}\int_{T_0}^{T_\alpha}\varepsilon^{E/PT}\delta T = \frac{A}{\beta}J(E_\alpha, T) \quad \text{(E5)}$$

where T_0 (K) is the initial temperature of the experiments, T_α (K) is the temperature measured at different preselected values of α during the reaction. β = dT/dt (K/min) is the heating rate with $T = T_0 + \beta t$, $g(\alpha)$ is the integral conversion function given in Table 3.

FR, KAS, FWO, and VA methods are popular mathematical models used for calculating kinetic parameters, thus they were used in this research. All the four methods were adopted in this study to calculate activation energies of coal pyrolysis with and without the use of catalysts.

Table 4 summarizes the adopted mathematical approaches for calculating the activation energy E [29–32]. Although being a more widely applicable method, the FR method suffers from some disadvantages as described by Vyazovkin, Golikeri and Luss. Since instantaneous rate values are employed, the method is numerically unstable [33]. Both FWO and KAS methods use certain kind of approximation formula for calculating the temperature integral, hence they may introduce unnecessary approximation errors, especially when E/RT is small. The Doyle's approximation used in FWO method can guarantee necessary accuracy only when 32<E/RT<45 [34]. Meanwhile, the Murray and White's approximation applied in the KAS method has a narrow accurate range of 20<E/RT<50. Hence, errors associated with the kinetic calculation by these two methods are dependent on the magnitude of variation of the activation energy with respect to the changing of the conversion rate [35,36]. Vyazovkin [37,38]

Table 3 – Most frequently used mechanism of solid state process.

Mechanism	Symbol	f(α)	g(α)
Order of reaction			
First-order	F_1	1-α	-ln(1-α)
Second-order	F_2	$(1-\alpha)^2$	$(1-\alpha)^{-1}$-1
Third-order	F_3	$(1-\alpha)^3$	$[(1-\alpha)^{-2}-2]/2$
Diffusion			
One-way transport	D_1	0.5α	α^2
Two-way transport	D_2	$[1-\ln(1-\alpha)]^{-1}$	α+(1-α) ln(1-α)
Three-way transport	D_3	$1.5(1-\alpha)^{2/3}[1-(1-\alpha)^{1/3}]^{-1}$	$[1-(1-\alpha)^{1/3}]^2$
Ginstling-Brounshtein equation	D_4	$1.5[(1-\alpha)^{1/3}]^{-1}$	$(1-2\alpha/3)-(1-\alpha)^{2/3}$
Limiting surface reaction between phases			
One dimensions	R_1	1	α
Two dimensions	R_2	$2(1-\alpha)^{1/2}$	$1-(1-\alpha)^{1/2}$
Three dimensions	R_3	$3(1-\alpha)^{2/3}$	$1-(1-\alpha)^{1/3}$
Random nucleation and nuclei growth			
Two-dimensional	A_2	$2(1-\alpha)\,[-\ln(1-\alpha)]^{1/2}$	$[-\ln(1-\alpha)]^{1/2}$
Three-dimensional	A_3	$3(1-\alpha)\,[-\ln(1-\alpha)]^{2/3}$	$[-\ln(1-\alpha)]^{1/3}$
Exponential nucleation			
Power law, n = 1/2	P_2	$2\alpha^{1/2}$	$\alpha^{1/2}$
Power law, n = 1/3	P_3	$3\alpha^{2/3}$	$\alpha^{1/3}$
Power law, n = 1/4	P_4	$4\alpha^{3/4}$	$\alpha^{1/4}$

found FWO and KAS methods involve a noticeable systematic error in the activation energy that does not appear in the FR method, which means FR methods are more reliable than those obtained from FWO and KAS methods. Unlike regression based methods like FR, FWO and KAS, Vyazovkin's methods (VO and VA) take a totally different mathematical approach through minimization. It can avoid systematic errors introduced by adopting approximation formula for the temperature integral, but it is known that the confidence interval for the activation energy calculated with this method is 10–20% which may make the result of little statistical significance.

Kinetic model

Master-plot methods have been successfully utilized for determining the mechanism of solid-state reaction, which is generally independent of the measured temperature conditions and kinetic parameters of the process. The kinetic function is determined by a master-plot method [23,36]. The method uses

$$g(\alpha) = \frac{AE}{\beta R} p(u) = \frac{AE}{\beta R} \int_{\infty}^{u} -\left(e^{-u}/u^2\right) du \tag{E6}$$

where $p(u)$ is the temperature integral, and p(u) = E/RT. Using a reference at point $\alpha = 0.5$, and based on E6, one gets

$$g(0.5) = \frac{AE}{\beta R} p(u_{0.5}) \tag{E7}$$

where $u_{0.5} = E/RT_{(0.5)}$. The following equation is obtained by dividing E6 by E7

$$\frac{g(\alpha)}{g(0.5)} = \frac{p(u)}{p(u_{0.5})}. \tag{E8}$$

The left side of the equation varies for different choices of kinetic function $g(\alpha)$, the right side of the equation can be calculated with data from experiments. The appropriate function $g(\alpha)$ is selected if the theoretical curve $\frac{g(\alpha)}{g(0.5)}$ matches best with the experiment curve $\frac{p(u)}{p(u_{0.5})}$ (i.e. $\sum_{\alpha}\left[\frac{g(\alpha)}{g(0.5)} - \frac{p(u)}{p(u_{0.5})}\right]^2$ is smallest and with high R^2 value). Some frequently used reaction functions are summarized in Table 3.

^{13}C NMR, FTIR, and XRD test methods

^{13}C Magic angle spinning nuclear magnetic resonance (MAS-NMR) data were acquired on a Bruker Avance III 600 NMR spectrometer, operating at Larmor frequencies of 600.2 MHz, 150.9 MHz, and 60.8 MHz for ^{13}C. A 5.0 mm triple resonance (^1H, ^{13}C, ^{15}N) E-free CPMAS Bio-solids probe was used, the temperature was held constant at 25.0 Degree Celsius and the spinning rate was 8000 Hz. Calibration was done using KBr and adamanatane. The samples were contained in 4 mm ZrO_2 rotors.^{13}C spectra were acquired using cross-polarization (CP) and the ramp.100 sequence for variable amplitude CP and the tppm13 sequence for ^{13} C. The recycle delay was 3 s for ^{13}C spectra. The contact time was 2000 us for ^{13}C experiments. Spectral widths were 502.0 ppm, and 8192 scans were acquired for the ^{13}C spectra.

FTIR spectroscopy and attenuated total reflectance (ATR) analyses of raw coal and coal chars produced in the fixed bed reactor system were recorded with a Nicolet Magna760 FTIR spectrometer (Thermo Scientific). The sample was subjected to 64 scans and measured at 4 cm^{-1} resolution in the wave number range of 4000–400 cm^{-1}. X-ray diffraction (XRD) analysis was performed on raw coal with and without catalysts and coal chars produced in the fixed bed reactor system in a Philips X'pert PW3040-MPD. Analyses were conducted using Cu Kα radiation (1.5406 Å) with 2θ ranging from 10° to 90° with 0.020° steps and at 40 KV/40 mA and a time/step of 0.05s.

Table 4 – Approximated equations of the kinetic methods [39].

	Approximated equation	Approach	y	x	k	A′
FR	$\ln(\beta d\alpha/dT) = -E(\alpha)/RT + (\ln A + \ln f(\alpha))$	$y = kx + A'^{a}$	$\ln(\beta d\alpha/dT)$	1/T	$-E(\alpha)/R$	$\ln A + \ln f(\alpha)$
KAS	$\ln\beta/T^2 = \ln(RA/E(\alpha)) - \ln g(\alpha)E/RT$	$y = kx + A'^{a}$	$\ln\beta/T^2$	1/T	$-E(\alpha)/R$	$\ln(RA/E(\alpha) - \ln g(\alpha)$
FWO	$\ln(\beta) = \ln\frac{AE}{Rg(\alpha)} - 5.331 - 1.052\frac{E}{RT}$	$y = kx + A'^{a}$	$\ln(\beta)$	1/T	$-1.052E(\alpha)/R$	$\ln\frac{AE}{Rg(\alpha)} - 5.331$
V	$\sum_{i=1}^{n}\sum_{j\neq i}^{n}\frac{J[E(\alpha),T_i]}{J[E(\alpha),T_j]} = \min$, with $J[E(\alpha),T] = \int_{t_\alpha-\Delta\alpha}^{t_\alpha}\exp(-E(\alpha)/RT)dt$	$E(\alpha) = \min^{b}$	–	–	–	–

[a] Calculation of E(α) is based on the linear regression of y and x to obtain slope k including E_α.
[b] Calculation of E(α) is based on the numerical minimization of function to get current value of E_α at the found minimum (no calculation of A is performed).

Results and discussion

Physical and chemical characteristics of raw coal with and without catalysts

^{13}C NMR was used to analyze the different carbon types in the raw coal structure. Generally, the solid-state ^{13}C NMR spectrum of coal can be divided into two main chemical regions: aromatic carbon (90–220 ppm) and aliphatic carbon (0–90 ppm) functional groups, respectively [39]. Different carbon functional groups can be represented by different chemical shifts, which are assigned into different carbon types, while the relative size of different peak areas indicates the relative contents of aromatic and aliphatic carbons in the coal sample.

The solid state ^{13}C NMR spectrum of raw coal is shown in Fig. 1. Using Peakfit V4.12 software, the spectrum was separated into 12 peaks using Gaussian and Lorentz methods, which represent different carbon types. The main chemical shift values and molar contents of different carbon types in raw coal are listed in Table 5 [40,41]. All kinds of carbon functional groups were found in the raw coal such as RCOR, $ROCH_3$, RCOOH, $-CH_2-$, and $R-CH_3$. In the aliphatic carbon region, the main peak centered at ~22 ppm attribute to aromatic CH_3 or CH_2, which could be a methylene and methyl group on the aromatic rings. A shoulder at ~16 and 32 ppm could be assigned to the CH_3 in the aliphatic functional group and methylene group in alicyclic moieties. In the aromatic carbon region, the protonated aromatic carbon at ~124 ppm is the most abundant. Noteworthy here, the obvious carbon peaks appeared at ~181 and 202 ppm, corresponding to carbonyl carbon in carboxyl, ketone, and aldehydes.

To clarify the carbon skeleton structure of the raw coal, some parameters were obtained and summarized in Table 6. The aromaticity f_a and aliphaticity f_{al} index are 29.98 and 59.14%, respectively. The raw coal contains 30 aromatic carbons and 59 aliphatic carbons per 100 carbon atoms. The χ_b index for raw coal is 0.07, which is close to the χ_b of benzene, suggesting that the average number of aromatic rings per cluster in the raw coal is 1 [40]. The average carbon number

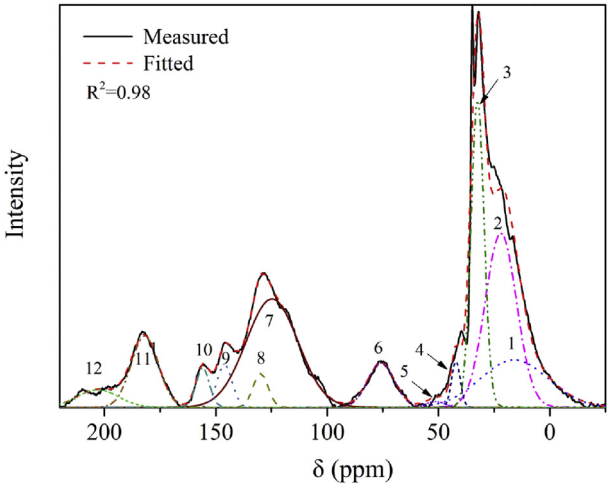

Fig. 1 – ^{13}CNMR spectra of raw coal.

Table 5 – Assignment of carbon functional groups for raw coal.

peak	chemical shift (ppm)	CT	symbol	mole content (%)
Aliphatic			f_{al}	
1	8–16	Aliphatic CH_3	f_{al}^{1}	13.18
2	16–22	Aromatic CH_3 or CH_2	f_{al}^{a}	22.42
3	22–36	Aliphatic CH_2 &CH	f_{al}^{2}	16.53
4	36–50	Tertiary or non-pronated carbon	f_{al}^{3}	1.66
5	50–60	Oxy-methylene	f_{al}^{O1}	0.46
6	60–90	Oxy-methine, oxy-quaternary	f_{al}^{O2}	4.89
Aromatic			f_{a}	
7	90–129	Protonated aromatic carbon	f_{a}^{H}	23.04
8	129–137	Bridgehead aromatic carbon	f_{a}^{b}	2.10
9	137–148	Alkylated aromatic carbon	f_{a}^{a}	2.67
10	148–164	Phenolic carbon	f_{a}^{p}	2.16
11	164–190	Carbonyl carbon in carboxyl	f_{a}^{c1}	7.96
12	190–220	Carbonyl in ketone and aldehydes	f_{a}^{c2}	2.92

Table 6 – Carbon structural parameters of raw coal determined by solid-state ^{13}C NMR.

Structural parameter	Symbol	Definition	value
Aromaticity index	f_a	$f_a = f_a^H + f_a^b + f_a^a + f_a^p$	29.98%
Aliphaticity index	f_{al}	$f_{al} = f_{al}^1 + f_{al}^a + f_{al}^2 + f_{al}^3 + f_{al}^{o1} + f_{al}^{o2}$	59.14%
Ratio of carbonyl carbon	f_a^c	$f_a^c = f_a^{c1} + f_a^{c2}$	10.88%
Mole percent of aromatic Bridgehead carbon	χ_b	$\chi_b = f_a^b/(f_a^H + f_a^a + f_a^p + f_a^b)$	0.07
Average methylene chain length	C_n	$C_n = f_{al}^2/f_a^a$	6.19
Substituted degree of aromatic ring	σ	$\sigma = (f_a^a + f_{al}^{o1} + f_{al}^{o2})/(f_a^H + f_a^a + f_a^p + f_a^b)$	0.27

(C_n) in methylene chain of raw coal is 6.19. The substituted degree σ of aromatic ring is 0.27, implying that the number of substituents on each aromatic ring is 1 or 2.

The FTIR spectra of the raw coal in the region 400–4000 cm^{-1} is given in Fig. 2. FTIR spectroscopy showed that the raw coal contains a variety of aromatic compounds substituted by aliphatic chains, oxygenated functional groups (such as phenolic hydroxyl, carbonyl, and carboxyl), and double bonds [42,43]. The presence of –OH bonds in the alcohol structures at 3700–3200 cm^{-1} and the –OH bending vibration in the carbonyl structures can be observed at 2500–3400 cm^{-1}. The C–H asymmetrical vibration of stretching in the region 2916–2936 cm^{-1} indicates the existence of $-CH_2$ alkane groups in the raw coal sample, while the

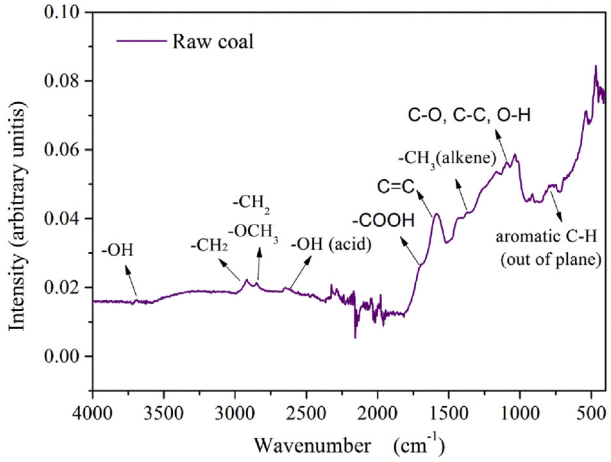

Fig. 2 – FTIR spectra of raw coal.

symmetrical vibration in the region 2843–2863 cm^{-1} indicates the existence of –CH alkane groups. Moreover, the C–H bending vibration in the region 1380–1460 cm^{-1} indicates the existence of $-CH_3$ alkane groups in the raw coal sample. The presence of C=O bonds in the carbonyl structures and C=C bonds can be observed at 1650 cm^{-1} and 1600 cm^{-1}, respectively. The C–O stretching vibrations in the region 1338–920 cm^{-1} indicates the existence of an alcohol, phenol, ether, anhydride, carboxylic acid, and ester. Furthermore, the absorption peak in the region 698–900 cm^{-1} indicates the presence of monocyclic, polycyclic, and substituted aromatic groups in the raw coal. The peak at 2360 cm^{-1} is attributed to CO_2 in the room atmosphere and system noise. To a certain extent, as a sub-bituminous ranked coal, the FTIR test results of PRB coal are consistent with coal structure of Hatcher molecule and NMR test results [44].

Fig. 3 presents the XRD spectrum of the raw coal with and without the use of catalysts. For all the samples, the strong characteristic peaks for the quartz (SiO_2) occur at 26.640°, 20.859°, 50.140°, and 59.960°, and those for kaolinite [$Al_4(OH)_8(Si_4O_{10})$] occur at 12.409°, 24.966°, 21.232°, and 20.380°. Also, a visible peak appears for 4% Na catalyst mixed with raw coal at 29.395°, 29.604°, 30.872°, and 16.494°, which are characteristic peaks of natron ($Na_2CO_3 \cdot 10H_2O$). The characteristic peaks for hematite (Fe_2O_3) occurs at 33.192°, 35.655°, 54.124°, and 49.505° for the raw coal sample with addition of 4% Fe catalyst. In addition, the peaks identified for the raw coal with uses of 3% Na– 1% Fe catalyst and peaks of natron and hematite are both presented. The major peaks and powder diffraction file (PDF) numbers of the species identified in the former XRD spectrum are listed in Table 7.

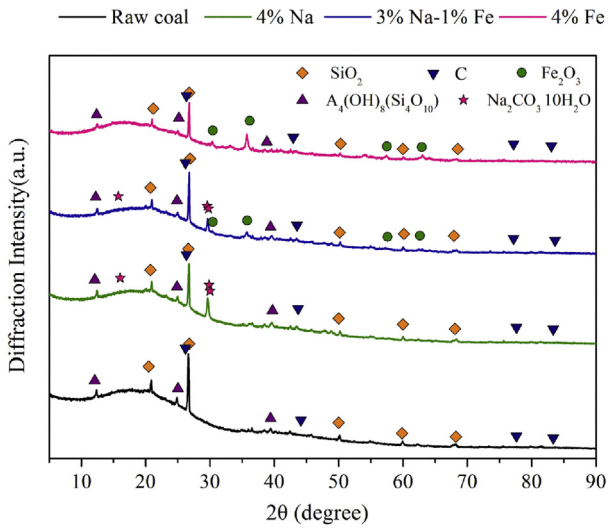

Fig. 3 – XRD patterns of raw coal with and without uses of catalysts.

Furthermore, the following structure parameters of aromatic layers can be obtained for the raw coal using XRD analysis [45,46]. The lateral size of the crystallite, L_a, the stacking height of the crystallize, L_c, the interlayer spacing, d_{002}, are observed and L_a, L_c can be determined using the conventional Scherrer Eq. E9 and E10 [47].

$$L_a = 1.84\lambda/B_a \cos(\theta_a) \quad \text{(E9)}$$

$$L_c = 0.89\lambda/B_c \cos(\theta_c) \quad \text{(E10)}$$

where λ is the wavelength of the X-ray radiation used, and B_a and B_c are the widths at half height of the (100) and (002) peaks, respectively. θ_a and θ_c are the corresponding scattering angles. It can be concluded that the d_{002}, L_a, and L_c for the raw coal sample are 0.3348 nm, 27.53 nm, and 42.71 nm, respectively.

Thermogravimetric analysis of the raw coal with and without the use of catalysts

Pyrolysis process

The TGA and derivative thermogravimetric (DTG) test profiles are presented in Fig. 4, and the corresponding characteristic parameters of pyrolysis are summarized in Table 8. The pyrolysis of the raw coal and coal with 3% Na–1% Fe,2% Na–2% Fe, 1% Na–3% Fe, and 4% Fe are proceeded in three steps. The temperature range of the first step of the raw coal and the catalyzed coal are all lower than 144 °C, in which the loss of water and light volatile compounds occur. The temperature ranges of the second step start from the end of the first step to 659 °C, 593 °C, 612 °C, 688 °C, and 650 °C, respectively. In the second step, the weight loss is attributed to the decomposition of organic compounds. The temperature ranges of the third step are from the ending temperature points of the second step to 900 °C, where carbonaceous residue decomposes gradually.

Meanwhile, the pyrolysis of the coal with the addition of 4% Na is different because it has four pyrolysis steps. The temperature range of the first step of the 4% Na coal is from the ambient temperature to 155 °C. The temperature ranges of the second, third, and fourth steps of 4% Na coal are 155–587 °C, 587–850 °C, and 850–900 °C, respectively. It should be noted that decomposition of carbonaceous solid residue and sodium carbonate should be the major factor in the third and last step of the pyrolysis, respectively.

Furthermore, $DTG_{(max)}$ of raw coal with 4% Fe is higher than those of the coal with addition of 4% Na, 1% Na–3% Fe, 3% Na–1% Fe, and 2% Na–2% Fe in the main pyrolysis stage, indicating that 4% Fe achieved the highest effect of the pyrolysis process, while 4% Na shows a higher effect than 1% Na–3% Fe and 3% Na–1% Fe does. In addition, the proportion of the mass weight loss of the raw coal (51.23%) is higher than that of the coal with addition of 4% Na, 3% Na–1% Fe, 2% Na–2% Fe, 1% Na–3% Fe, and 4% Fe catalysts, 48.97%, 47.86%, 47.33%, 48.26%, and 49.43% respectively, under the same experimental condition. Also, the weight loss of raw coal sample with 4% Fe is higher than those of the coals, indicating that 4% Fe achieved the highest effect on coal conversion, while 4% Na and 1% Na–3% Fe show a higher effect than 3% Na–1% Fe and 2% Na–2% Fe does. The results indicate that addition of a catalyst improves the pyrolysis rate of the raw coal sample.

Effect of heating rate

The DTG curves of the raw coal and the coal with 4% Na, 4% Fe and 1% Na–3% Fe at several β s (10, 20, and 50 °C/min) are shown in Fig. 5. With the heating rate increasing, the temperature of the maximum weight loss rate of the sample shifts toward higher temperatures, resulting from the fact that the temperature of particles was slightly lower than that of the furnace, which indicates that a temperature gradient (thermal lag) existed between the furnace and the sample temperature. On the other hand, a higher heating rate will reduce the pyrolysis time for a given amount of coal sample. To eliminate the thermal lag, the sample of the coal powder should be grounded as finely as possible, which can increase the surface area of the particles and consequently increase the heat transfer rate between the sample powder and the crucible.

Table 7 – Peaks and PDF numbers of the species identified in the XRD spectra.

Name	Chemical Formula	Main peaks (2θ)	PDF number
Quartz	SiO_2	26.640°,20.859°,50.140°,59.960°	99–0088
Kaolinite	$Al_4(OH)_8(Si_4O_{10})$	12.409°,24.966°,21.232°,20.380°	99–0067
Hematite, syn	Fe_2O_3	33.192°,35.655°,54.124°,49.505°	89–0599
Natron, syn	$Na_2CO_310H_2O$	29.395°,29.604°,30.872°,16.494°	15–0800
Graphite	C	26.603°,44.665°,83.845°,77.697°	99–0057

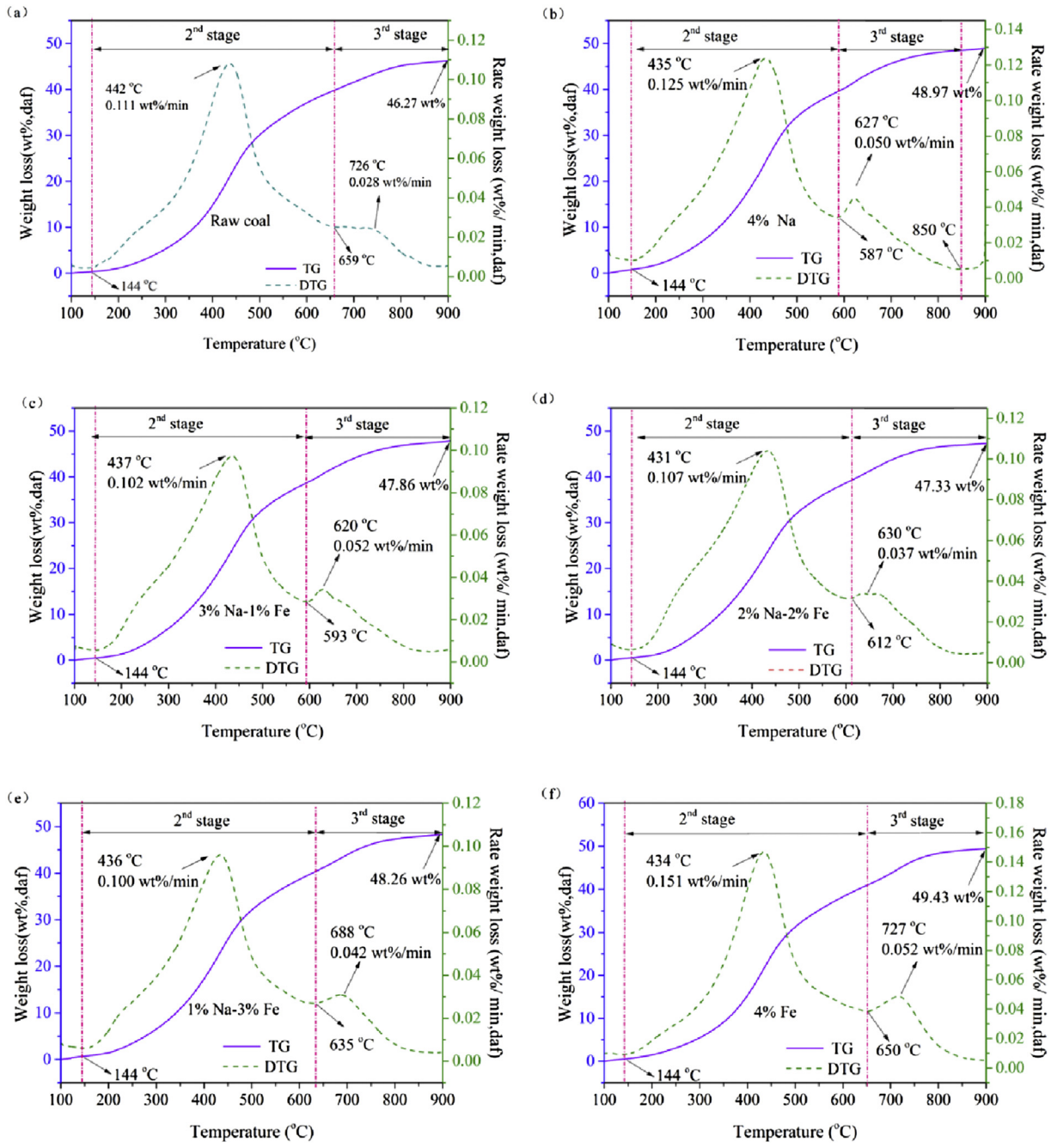

Fig. 4 – TG and DTG profiles of coals with and without uses of catalysts [TGA operation conditions-temperature: 900 °C; heating rate: 10 °C/min; flow rate of carrier gas N_2; 60 ml/min].

Table 8 – Characteristic parameters of coal pyrolysis with and without uses of catalysts.

Sample	StepII				Step III				Step IV		Residue (wt.%)
	T_1 (°C)	T_f (°C)	T_p (°C)	DTG_{max} (%/°C)	T_1 (°C)	T_f (°C)	T_p (°C)	DTG_{max} (%/°C)	T_1 (°C)	T_f (°C)	
Raw coal	144	659	442	0.111	659	900	726	0.028	–	–	46.27%
4% Na– 0% Fe	155	587	435	0.125	587	850	627	0.050	850	900	48.97%
3% NA-1% Fe	144	593	437	0.102	593	900	620	0.052			47.86%
2% Na–2% Fe	144	612	431	0.107	612	900	630	0.037			47.33%
1% Na–3% Fe	144	635	436	0.100	635	900	688	0.042			48.26%
0% Na –4% Fe	144	650	434	0.151	650	900	727	0.052	–	–	49.43%

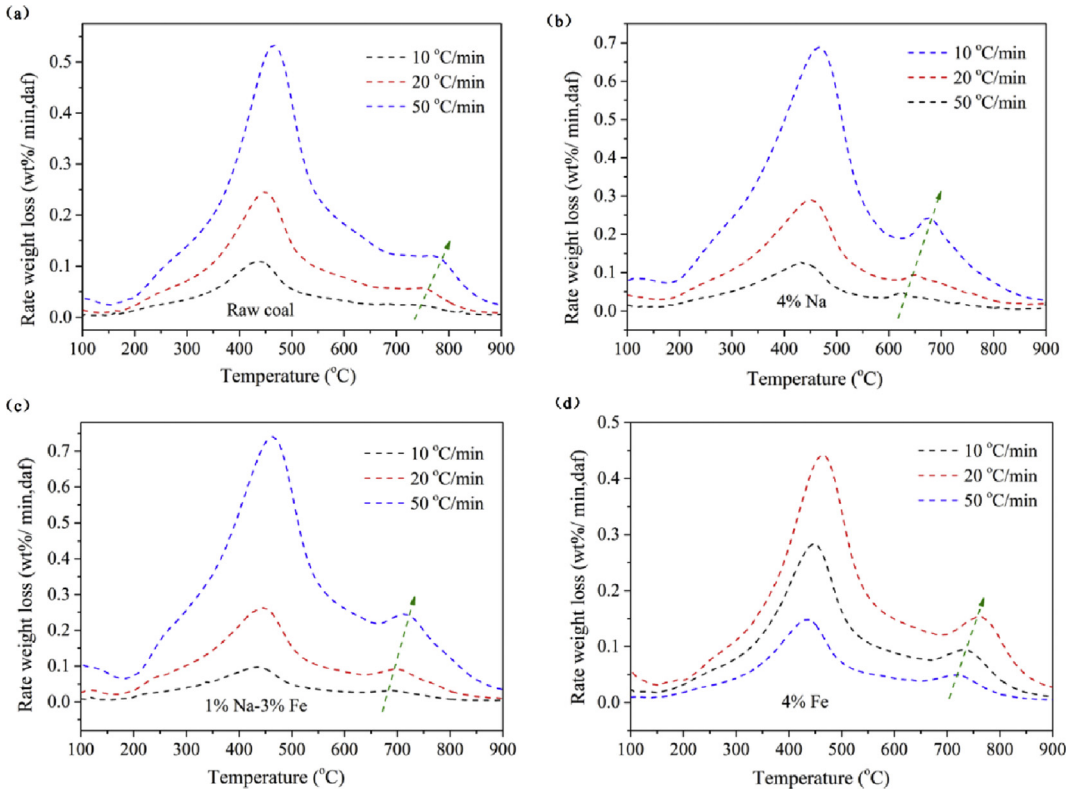

Fig. 5 – DTG profiles for coal with and without catalyst addition at several β s [a: raw coal; b: 4% Na; c: 1% Na–3% Fe; d: 4% Fe; TGA operation conditions-temperature: 900 °C; flow rate of carrier gas N_2: 60 ml/min].

Effect of catalysts

Fig. 6 shows the TGA and DTG curves obtained for the coal samples with and without the use of catalysts at a heating rate of 10 °C/min. All data are calculated based on a dry and ash-free basis (DAF). The TG curves of the pyrolysis of the raw coal samples with and without the use of catalysts have the same trend. Obviously, the weight loss of the raw coal sample with 4% Fe is higher than those of the coal with the addition of 3% Na–1% Fe, 2% Na–2% Fe, 1% Na–3% Fe, and 4% Na, indicating that 4% Fe achieved the highest effect on coal conversion, while 4% Na and 1% Na–3% Fe shows a higher effect than 3% Na–1% Fe and 2% Na–2% Fe. Meanwhile, the $DTG_{(max)}$ of the raw coal with the addition of 4% Fe and 4% Na are obviously higher than those of the coal with addition of 2% Na–2% Fe, 1% Na–3% Fe, and 3% Fe. Thus, samples for raw coal with the addition of 1% Na–3% Fe and 3% Na–1% Fe catalysts sample were selected to study the effect of composite catalysts on the pyrolysis characteristics and kinetic analysis of raw coal.

Kinetic analysis

(1) Determination of the activation energy

In this study, FR, KAS, FWO and VA methods are applied for determining the activation energy, the obtained activation

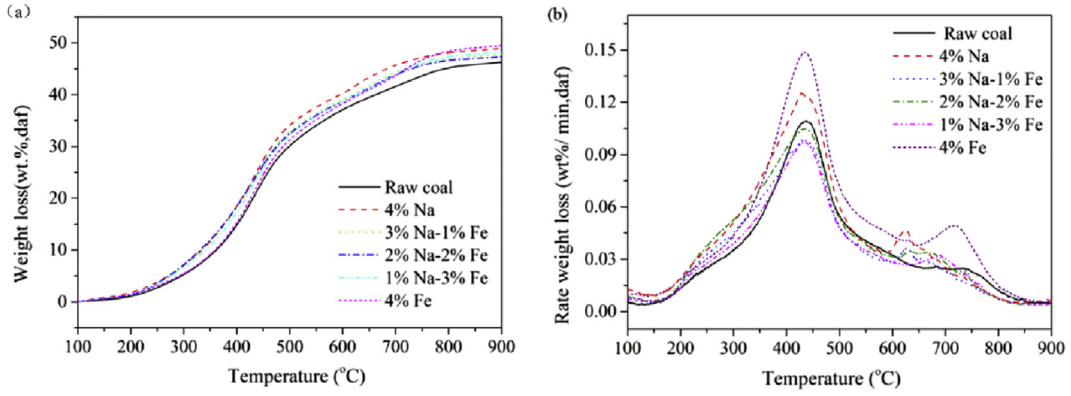

Fig. 6 – Effect of catalysts on coal pyrolysis under the heating rate is 10 °C/min [TGA operation conditions-temperature: 900 °C; isothermal time: 10 min; flow rate of carrier gas N_2: 60 ml/min].

energies for the raw coal with and without the use of catalysts at $\beta = 10, 20, 30, 40$, and 50 °C/min with selected values of α ($0.20 \leq \alpha \leq 0.90$)are presented in Table 9 As shown in Fig. 7, the four different methods give consistent results. R^2 of curves are higher than 0.9 when $0.2 \leq \alpha \leq 0.9$, indicating the four methods work well for the collected data over this range. Meanwhile, most of the E value deviations obtained by the four methods are all within 5% of the lowest E value. Therefore, it is properly assumed that the results are acceptable.

Generally, if the activation energy value remains constant, probably only one reaction exists. However, if the E values increase during the progression of the reaction, competitive parallel reactions could occur. The activation energy distribution with increasing α ($0.2 \leq \alpha \leq 0.9$) is summarized in Table 9 and Fig. 7. Results show that with the proceeding of pyrolysis, activation energy values of the raw coal increase gradually, indicating that competitive parallel reactions occur. The average E values are 271.02 kJ/mol by KAS, 269.76 kJ/mol by FWO, 279.68 kJ/mol by FR, and 277.36 kJ/mol by VA. When $\alpha > 0.70$ (temperature around 560 °C), a dramatic change in E values occurred with an increase of 100 kJ/mol. This increase suggests the main pyrolysis reaction happened in this stage. This result should be attributed to the decomposition of oxygenated functional groups of raw coal and its primary pyrolysis.

For the raw coal with the use of catalysts, the average E values are from 220 to 480 kJ/mol. The addition of 4% Fe catalyst decreases the activation energy over the main range

Table 9 – The E values at $\beta = 10,20,30,40$ and 50 °C/min by KAS,FWO, FR and VA methods.

Samples	α	KAS method		FWO method		FR method		VA method
		E	R^2	E	R^2	E	R^2	
Raw coal	0.2	198.29	0.99111	198.60	0.99198	204.35	0.99628	196.93
	0.3	201.15	0.99445	201.98	0.99506	206.87	0.9988	201.53
	0.4	207.69	0.98503	207.93	0.9851	212.67	0.98314	222.46
	0.5	207.82	0.98498	207.93	0.9851	218.45	0.98371	233.56
	0.6	238.87	0.97547	239.18	0.97789	248.29	0.95788	244.01
	0.7	270.88	0.94552	270.38	0.95047	288.05	0.9361	276.37
	0.8	389.60	0.99063	386.36	0.98268	406.45	0.98268	389.88
	0.9	453.84	0.90824	445.73	0.92874	452.28	0.92874	454.17
	Average	271.02	–	269.76	–	279.68	–	277.36
4% Na	0.2	263.58	0.98348	260.26	0.86494	258.18	0.98686	270.82
	0.3	231.64	0.98638	230.61	0.95603	228.95	0.97859	233.19
	0.4	242.94	0.98806	241.88	0.98855	244.25	0.98652	244.14
	0.5	243.17	0.8942	242.55	0.91933	249.61	0.99087	243.98
	0.6	257.25	0.97993	256.37	0.98855	275.50	0.9719	258.79
	0.7	312.18	0.93259	309.20	0.92293	342.26	0.91772	319.74
	0.8	371.23	0.92972	365.51	0.95446	349.89	0.94209	374.77
	0.9	368.77	0.79634	364.93	0.86096	382.05	0.73482	382.87
	Average	286.35	–	283.91	–	291.34	–	291.04
3% Na–1% Fe	0.2	240.65	0.94253	238.45	0.94705	245.17	0.94163	243.35
	0.3	239.15	0.98162	237.71	0.98324	238.44	0.98596	239.96
	0.4	226.51	0.91889	226.25	0.92629	233.82	0.93096	235.15
	0.5	242.27	0.99071	241.69	0.9916	243.62	0.99478	242.63
	0.6	258.61	0.99324	257.68	0.99389	273.59	0.99305	258.56
	0.7	330.74	0.99867	326.92	0.99878	371.09	0.99702	330.60
	0.8	440.90	0.99065	432.84	0.99124	463.53	0.99061	442.26
	0.9	472.11	0.9918	463.93	0.99232	482.91	0.98985	474.52
	Average	306.37	–	303.18	–	319.02	–	308.38
1% Na–3% Fe	0.2	223.64	0.99082	222.43	0.99165	221.24	0.98618	235.66
	0.3	217.81	0.9973	217.58	0.99757	221.36	0.99942	216.96
	0.4	219.08	0.99062	219.31	0.99159	224.06	0.99255	235.72
	0.5	237.03	0.99921	236.61	0.99939	248.47	0.99837	252.44
	0.6	254.71	0.99753	254.10	0.99773	271.18	0.99512	251.14
	0.7	297.94	0.96398	295.98	0.96691	294.16	0.94546	300.33
	0.8	343.78	0.99342	340.80	0.99398	371.99	0.99529	365.06
	0.9	404.37	0.99366	399.86	0.99411	420.22	0.99834	399.66
	Average	274.79	–	273.33	–	284.08	–	282.12
4% Fe	0.2	223.87	0.94187	222.97	0.94694	221.27	0.95642	226.38
	0.3	215.78	0.95287	215.93	0.95742	230.24	0.98723	215.02
	0.4	232.09	0.99603	231.87	0.9964	237.28	0.99691	233.11
	0.5	233.16	0.98621	233.31	0.98755	238.62	0.98905	235.31
	0.6	242.20	0.99692	242.45	0.99725	247.19	0.99601	242.42
	0.7	265.45	0.98837	265.48	0.98954	267.29	0.99199	265.87
	0.8	279.03	0.97674	279.71	0.97916	284.88	0.96312	281.99
	0.9	309.17	0.96118	309.80	0.9651	328.67	0.97066	312.86
	Average	250.09	–	250.19	–	256.93	–	251.62

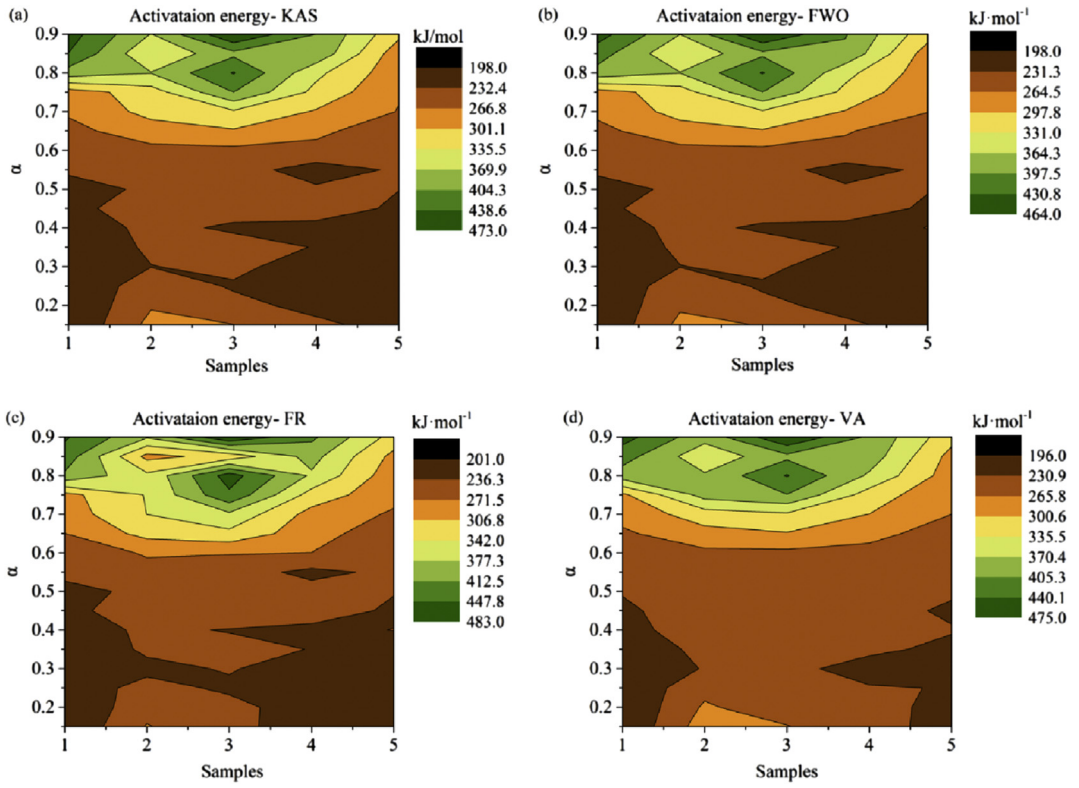

Fig. 7 – Variation profiles of E versus α for raw coal with and without uses of catalysts; (a) by KAS, (b) by FWO, (c) by FR, (d) by VA.

of the pyrolysis process when $\alpha > 0.50$ (temperature higher than 500 °C), while the addition of 4% Na decreases the activation energy in the 3rd step of the raw coal pyrolysis when $\alpha > 0.80$ (temperature higher than 650 °C) compared with the E values of DAF coal at the same conversion. The averaged E value of raw coal pyrolysis with the addition of 4% Fe (251.62 kJ/mol by VA) is lower than that of the raw coal (277.36 kJ/mol by VA), while the average E value of raw coal pyrolysis with the use of 4% Na (291.04 kJ/mol by VA) is higher than that of raw coal (277.36 kJ/mol by VA). As for the composite catalysts, the average E value of 3% Na–1% Fe (308.38 kJ/mol by VA) is higher than that of 1% Na–3% Fe (282.12 kJ/mol by VA). For 1% NA-3% Fe, the E values are lower than that of raw coal at $\alpha > 0.80$, while the E value of 3% Na–1% Fe are higher than that of raw coal. In other words, the average E value of the raw coal with the use of 4% Fe decreased by 10% compared with that of the raw coal. Thus, the addition of 4% Fe can promote the raw coal pyrolysis, while the addition of 4% Na inhibits coal pyrolysis for the whole process. The addition of $FeCO_3$ can decrease the activation energy value of the raw coal compared with individual use of Na_2CO_3. The mechanism associated with the fact is studied in the next section.

As seen in Fig. 8a, by using the considered iso-conversional methods, all curves for E as a function of α share the same trend. For the same sample, the calculated values of apparent activation energy for FR differential and the VA nonlinear methods are higher than those of E values for the KAS and FWO integral methods. Meanwhile, the calculated E values obtained by the KAS are close to the ones obtained from the FWO and, the calculated E values by the FR are similar with the ones obtained from the VA. The same trend is also established for the calculated average E. The significant differences between the above methods are due to the way the relations of integral methods are derived [48]. Compared to linear integral procedures, the nonlinear VA method was found to be very accurate with the relative error in E values is practically independent of values of E/RT [49]. The dependence of iso-conversional intercepts (FR, KAS, and FWO) on the degree of conversion α is presented in Fig. 8b. The results show the highest average value of iso-conversional intercept is given by FWO method, followed by the FR and the KAS method. In summary then, the nonlinear VA methods appears to provide the most reasonable values; albeit, more computational effort is involved for the range of α in our experimental data.

(2) Determination of pre-exponential factor and reaction order

Using the average E values calculated by the VA method, along with the temperature measured versus conversion α, p(u) can be obtained according to the Equation $p(u) = \int_u^\infty \frac{e^{-x}}{x^2} dx$ and $u = \frac{E}{RT(\alpha)}$ from direct numerical integration. Fig. 9a and b are the experimental master-plots of $p(u)/p(u_{0.5})$ against α at β = 10, 20 and 50 °C/min for the raw coal with and without the

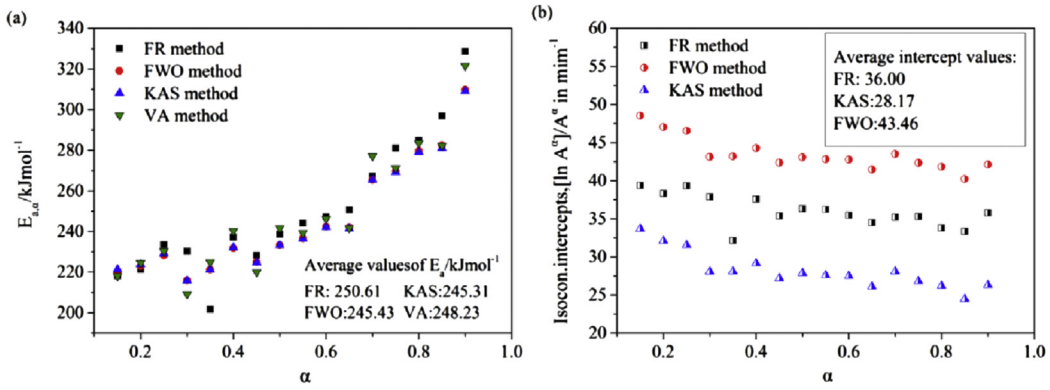

Fig. 8 – Variation profiles of E and isconversional intercepts values versus α for raw coal with addition of 4% Fe by FR, FWO, KAS and FWO isconversional methods; (a) E values, (b) [$\ln A_\alpha$]/A_α.

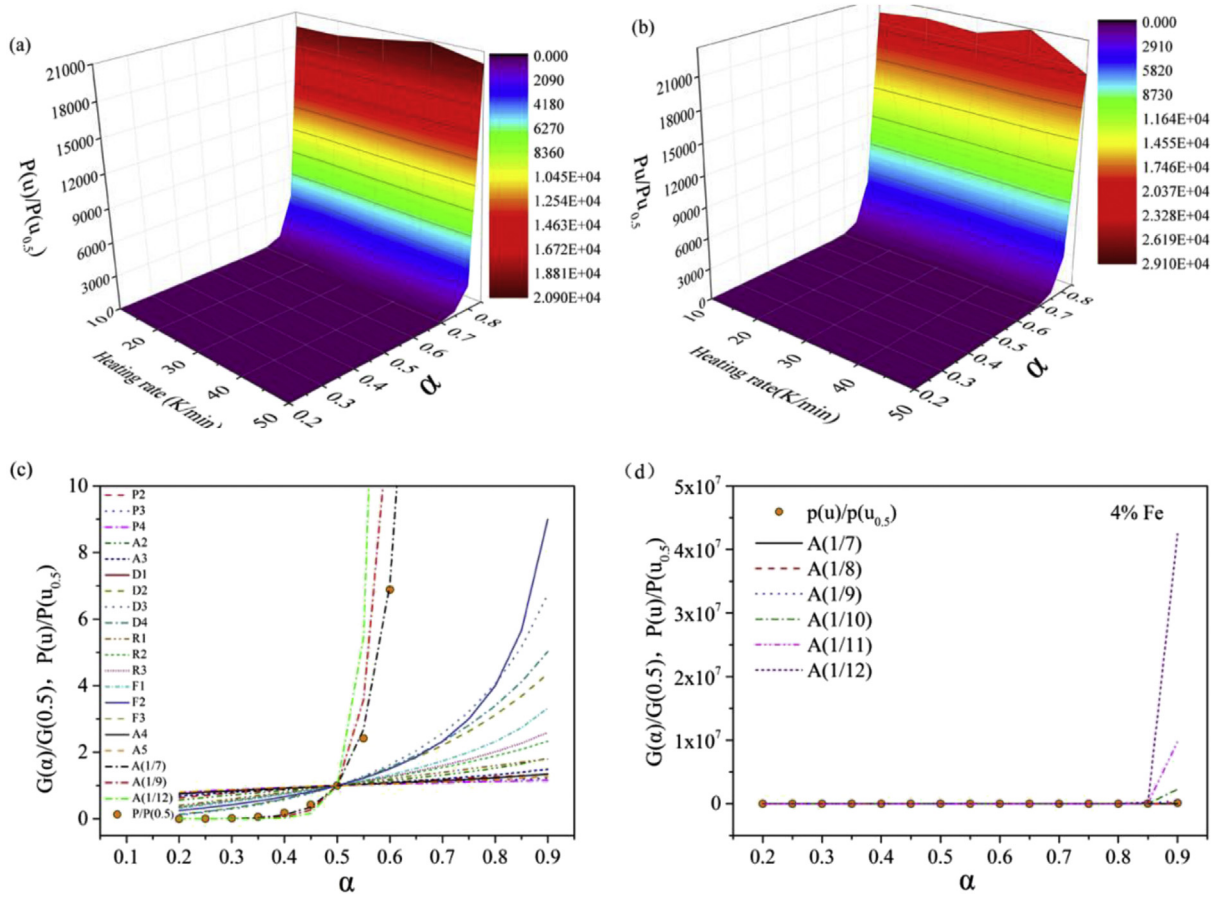

Fig. 9 – Plots of P(u)/P($u_{0.5}$) versus α for (a) raw coal and (b) raw coal with addition of 4% Fe; (c) theoretical master-plots of g(α)/g (0.5) against α and experimental master-plots of P(u)/P($u_{0.5}$) against α for raw coal at heating rate β = 10 °C/min; Plots of G(α)/G (0.5)/[P(u)/P($u_{0.5}$)] against α for raw coal at heating rate β = 10 °C/min.

use of 4% Fe. The results indicate that the values of p(u)/p($u_{0.5}$) at different heating rate are identical when α is lower than 0.8, suggesting that the kinetics of the raw coal with and without a catalyst could be described by a single reaction model.

Fig. 9c shows experimental master-plots of p(u)/p($u_{0.5}$) at a heating rate β = 10 °C/min and theoretical master-plots g(α)/g (0.5) for different solid-state reaction models of raw coal. The comparison between the experimental and theoretical results indicates that the present master-plots could not match the experimental ones; however, the theoretical master-plots in A_n model (Random nucleation and nuclei growth) with order less than 1 seems to best match the trend of our experimental data. To further determine the reaction order n and pre-exponential factor A, two different regression methods based on the original master-plot methods are implemented in MATLAB. The detailed information is included in the

support information. The most appropriate values of n and corresponding pre-exponential factor A are listed in Table 10. The left column of the Table is by applying regression method II with activation energy E calculated from the VA method. The right column of the table uses the same method but with E calculated from FR method as a comparison. Results are n = 0.12, 0.11, 0.10, 0.11, 0.13 and lnA = 41.86, 45.17, 47.72, 42.99, 37.26 for the raw coal and raw coal with addition of 4% Na, 3% Na–1% Fe, 1%Na–3% Fe and 4% Fe, respectively. Hence, it can be assumed that as the PRB coal is heated to certain temperature, i.e., the softening point, coal melts and begin to soften. Hence, a thermally-derived plasticizing agent, known as metaplast, is reached. Further temperature increases, the metaplast decomposes and polymerizes to form more stable and aromatic products as well as light gaseous volatiles. Since vaporized metaplast no longer functions as a plasticizing agent, metaplast vapor within the bubbles and metaplast escapes, and the particles are counted as coal tar and the coal resolidifies [50].

Fixed-bed pyrolysis of the raw coal with and without the use of catalysts

Gas evolution analysis

Fig. 10 showed the main gas evolution of PRB coal pyrolysis with and without use of catalysts which includes H_2, CO, CH_4 and CO_2. All adopted catalysts can enhance or significantly enhance the yield of H_2 and CO_2 and decrease the yield of CO at the studied temperature range. The Na based catalyst is more effective than Fe based ones in increasing H_2 yield. When the pyrolysis temperature is lower than 700 °C, Fe based catalysts is more effective than Na one in decreasing CO yields, while the CH_4 yield produced by raw coal pyrolysis with use of Fe-based catalysts is remarkable increased when the pyrolysis temperature is higher than 700 °C.

XRD and FTIR analysis for coal chars

Fig. 11 shows XRD analysis for chars produced by raw coal pyrolysis with and without use of catalysts. As seen in Fig. 11, no characteristic iron peaks are found in the coal chars produces by raw coal pyrolysis while the characteristic peaks of magnetite (Fe_3O_4) in the char obtained from raw coal pyrolysis with 4% Fe at 500 °C are present at 35.479°, 62.622° 30.121° and 57.026°. When pyrolysis temperature is 600 °C, characteristic peaks of magnetite disappear and characteristic peaks of metallic iron are present at 44.673°, 65.021° and 82.333°. This indicates that the initial magnetite was transformed into iron under the given reaction conditions. This trend becomes more obvious for the sample obtained at 700 °C at which the main characteristic peaks of iron at 44.673° are higher and sharper than those with 600 °C. When pyrolysis temperature is increased to 800 °C, the intensity of the characteristic peaks of iron starts to decrease, while the peaks of the formed cementite (Fe_3C) center at 45°, which indicates that the partly metallic iron was transformed into cementite. The major peaks and powder diffraction file (PDF) numbers of the species identified in the former XRD spectra are listed in Table 11.

As seen in Fig. 12, the main difference for the coal char samples with and without uses of catalysts appear in the region 1650 cm^{-1},1450 cm^{-1}, 880 cm^{-1} and in the region 1338-920 cm^{-1}. No peak in the region 1650 cm^{-1} was found for raw coal char sample indicating oxygen functional group corresponding to –C=O in the carbonyl/carboxyl structure should be removed as volatiles at 700 °C during raw coal pyrolysis, while it appears at coal char samples produced by raw coal with addition of 4% Na, 3% Na–1% Fe, indicating the C–O–M (M represents alkalis) resulting in sodium phenolate(–C–O–Na) was formed [51].

Proposed catalytic pyrolysis mechanism of raw coal with use of Na–Fe composite catalysts

As a sub-bituminous coal, the PRB coal has a variety of oxygenated group in its structure. As shown in the NMR and FTIR results for raw coal, –COOH, $-OCH_3$, –C=O, and –OH were all presented. Generally, coal pyrolysis proceeds in three steps: dry outgassing, primary pyrolysis, and secondary pyrolysis [52]. During primary pyrolysis, the weakest bonds in

Table 10 – n and A obtained at β = 10, 20 and 50 °C/min by Regression Method II.

Samples	Averaged E decided by VA method					Averaged E decided by FR method				
	β	R^2	n	lnA (min^{-1})	lnA average value(min^{-1})	β	R^2	n	lnA(min^{-1})	lnA average value(min^{-1})
Raw coal	10	0.9695	0.12	41.80	41.86	10	0.9695	0.12	42.17	42.22
	20	0.9706		41.90		20	0.9706		42.26	
	50	0.9699		41.89		50	0.9699		42.24	
4% Na	10	0.9796	0.11	45.22	45.17	10	0.9796	0.11	45.27	45.21
	20	0.9808		45.01		20	0.9808		45.06	
	50	0.9828		45.27		50	0.9828		45.31	
3% Na–1% Fe	10	0.9814	0.10	47.87	47.72	10	0.9814	0.10	49.58	49.40
	20	0.9916		47.44		20	0.9916		49.12	
	50	0.9840		47.84		50	0.9840		49.50	
1% Na–3% Fe	10	0.9773	0.11	43.01	42.99	10	0.9773	0.11	43.32	43.30
	20	0.9800		42.96		20	0.9800		43.26	
	50	0.9802		43.00		50	09802		43.30	
4% Fe	10	0.9664	0.13	37.25	37.26	10	0.9664	0.12	38.07	38.07
	20	0.9690		37.31		20	0.9690		38.12	
	50	0.9679		37.23		50	0.9679		38.02	

The averaged E value decided by VA method and FR method.

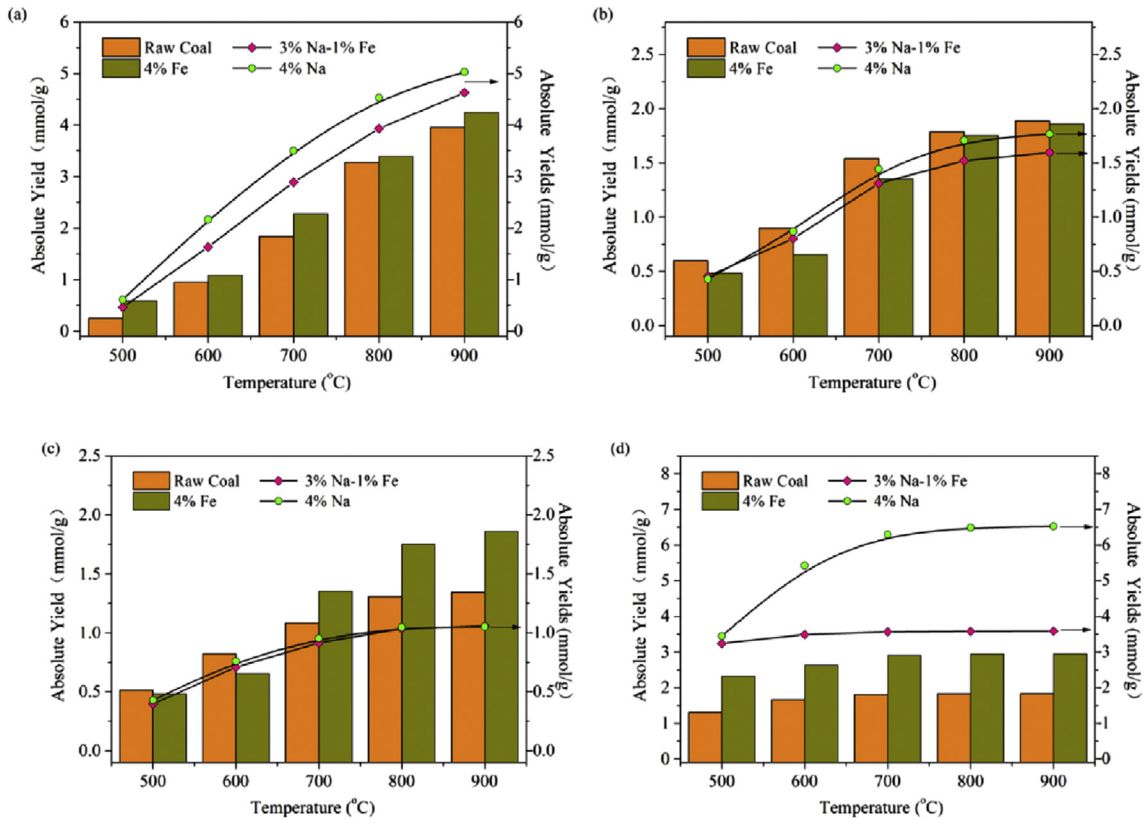

Fig. 10 – Main gas evolution of PRB coal pyrolysis with and without use of catalysts (a. H_2; b. CO; c. CH_4; d. CO_2).

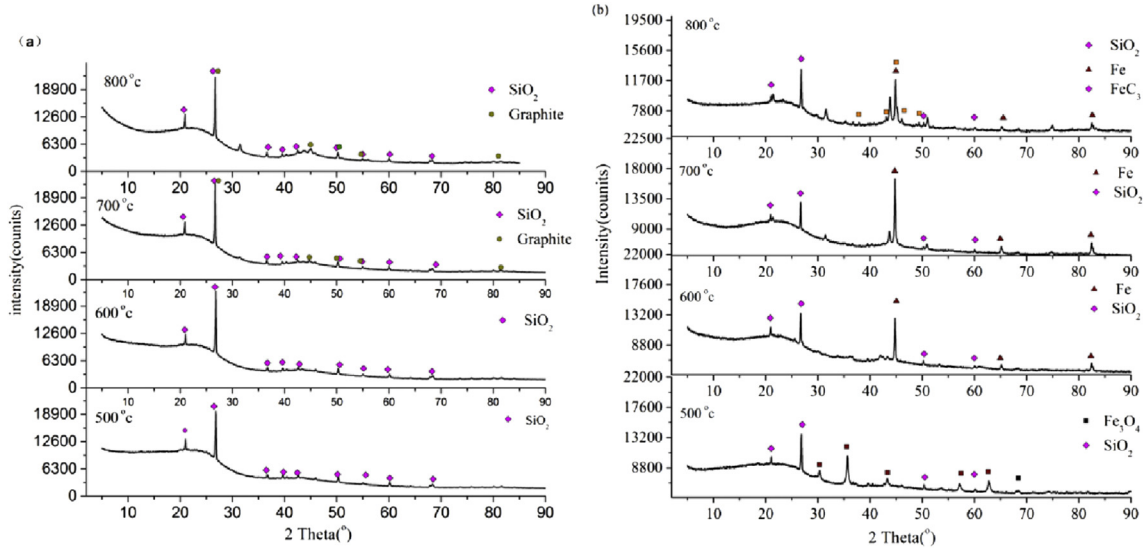

Fig. 11 – XRD analysis for chars produced by raw coal pyrolysis with uses of catalysts. (a) raw coal char, (b) coal chars produced by raw coal with use of 4% Fe catalyst.

the coal are broken and molecular fragments (depolymerization) are produced and volatiles, such as coal tar, CO_2, CO, light aliphatic gases, and other species are released. During this stage, the thermal stabilities of functional groups in PRB coal are displayed in the following order: OH > –O– > C–H ≈ aliphatic C–H > substituted aromatic ring > C=O > COOH, decarboxylation and decarbonylating reaction happened [53].

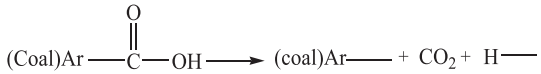

(R2)

Table 11 – The major peaks and PDF numbers of the species identified in XRD spectra for coal chars.

	Main peaks (2θ)	PDF number
SiO_2	26.640, 20.859, 50.140,59.960	99–0088
Kaolinite	12.409, 24.966, 21.232, 20.380	99–0067
Fe_2O_3	33.161, 35.629, 54.073, 49.463	99–0060
Fe_3O_4	35.479, 62.622, 30.121, 57.026	88–0866
Fe	44.673, 82.333,65.021	06–0696
Fe_3C	44.997, 42.893, 43.763, 44.575	65–2411
Graphite	26.603,44.665,83.845, 54.793	99–0057

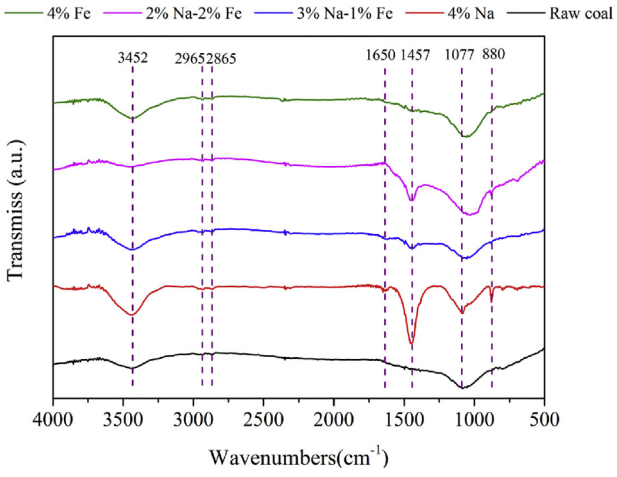

Fig. 12 – FTIR analysis of coal char produced by raw coal pyrolysis with and without use of catalysts.

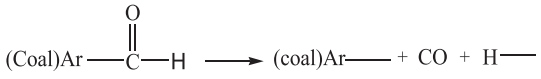

(R3)

During the secondary pyrolysis, additional gases were released, accompanied by mature coal char produced by the cross-linking reaction [54]. During this stage, CH_4 evolution was a result of cleavage of the methyl group, CO evolution was a result of an ether link and H_2 was from the ring condensation reaction [55].

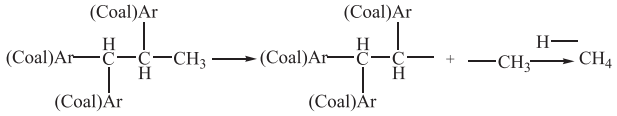

(R4)

(R5)

When Na_2CO_3 is used in coal pyrolysis as a catalyst at a low temperature, Na^+ is associated with $-COO^-$ and $-OH$ group to form "C–O–Na" clusters as shown in FTIR test results for coal char produced by raw coal with use of Na-based catalysts, the following reaction happened. More hydrogen was formed, which is in accordance with the result from fixed-bed pyrolysis analysis.

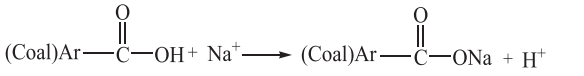

(R6)

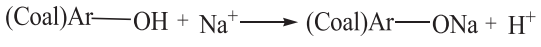

(R7)

The "C–O–Na" structure strengthen the force between the coal macromolecule structure and the density of coal. Therefore, more energy is needed to release volatiles such as tar and gas during coal pyrolysis. Meanwhile, based on the research by Liu et al. [56], it is possible that the $-COONa$ can increase the activation energy of decomposition of phenolic hydroxy and ether bonds. These analyses are in accordance with the activation energy, which increases for raw coal with the addition of 4% Na in low temperatures. When the temperature gets higher with the release of CO_2, Na originally bonded with $-COOH$ group in the coal matrix will be bonded to coal/coal char matrix.

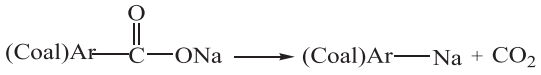

(R8)

As the temperature further increases, the new bond (Coal) Ar-Na becomes less stable and will be broken again to combine new free radicals to form more stable bonds. Meanwhile, based on the research by Li et al. [5,57], during this process, some of the aliphatic components in the coal tar precursors were cracked into gas and some of the larger aromatic ring systems were charred. These analyses agree with the observation that the activation energy of raw coal with the use of Na_2CO_3 decreases when $\alpha > 0.80$ (temperature higher than 650 °C), indicating that Na_2CO_3 can promote the coal charring process.

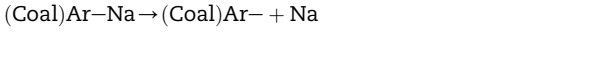

(R9)

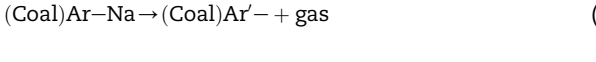

(R10)

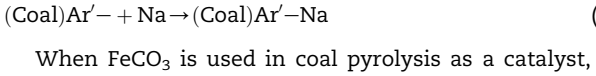

(R11)

When $FeCO_3$ is used in coal pyrolysis as a catalyst, it is found that the raw coal with 4% Fe mainly contains Fe_2O_3 according to XRD test for raw coal, which results from the decomposition of $FeCO_3$ when it is calcined at 250 °C. It is known that tar, coal char, and incondensable gas (H_2, CO, CO_2, and CH_4) are the main products of coal pyrolysis. Based on the XRD results for coal chars produced by raw coal with use of 4% Fe in the fixed bed reaction system, with the increasing of pyrolysis temperature, the chemical formats of iron in coal chars are given as follows: Fe_3O_4,FeO, Fe and Fe_3C.Combining the gas evolution results that with the use of Fe-based catalysts, the CO yields decreased and the CH_4 yield produced by raw coal pyrolysis with use of Fe-based catalysts is remarkable increased when the pyrolysis temperature is higher than 700 °C, the following reaction mechanism is given.

When the temperature is in the range of 400–500 °C, the Fe_2O_3 could be reduced as follows:

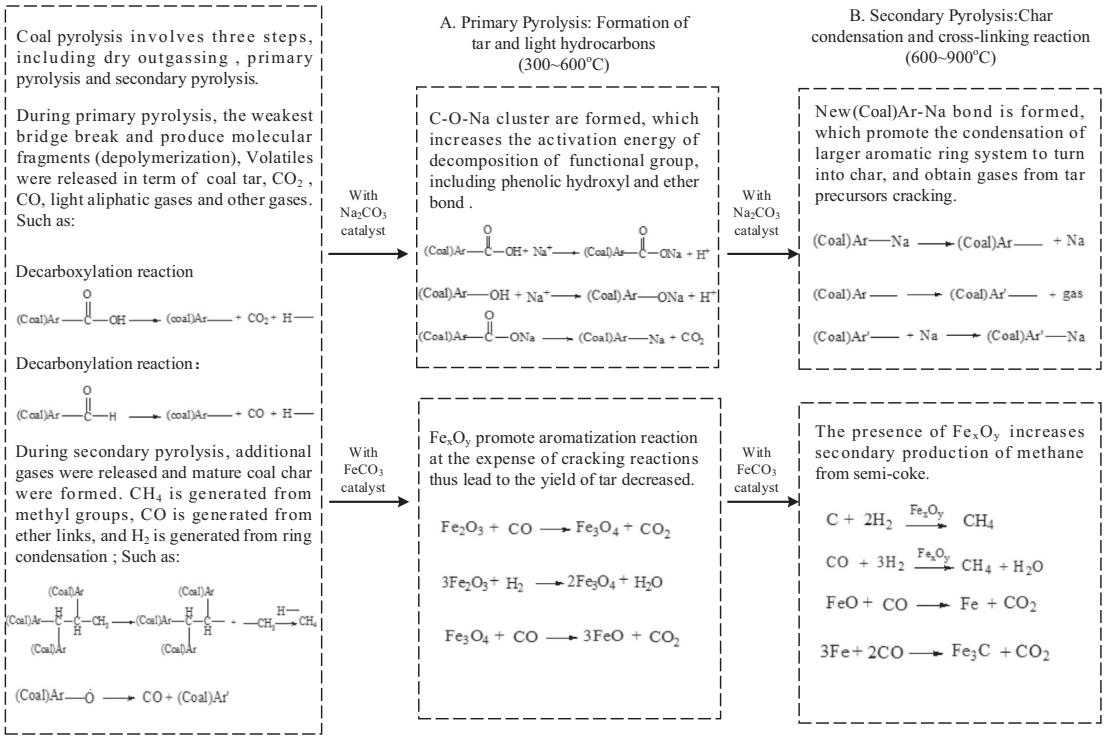

Fig. 13 – The Integrated catalytic mechanism of raw coal pyrolysis with and without uses of Na–Fe catalysts.

$$3Fe_2O_3 + CO \rightarrow 2Fe_3O_4 + CO_2 \quad \text{(R12)}$$

$$3Fe_2O_3 + H_2 \rightarrow 2Fe_3O_4 + H_2O \quad \text{(R13)}$$

When temperature is higher than 500 °C, Fe_3O_4 could also be reduced to FeO/Fe by CO. FeO can also be generated from R13 occurring in the range of 500 °C–600 °C, while Fe is the product of further reduction of FeO with CO with the temperature higher than 600 °C.

$$Fe_3O_4 + CO_2 \rightarrow 3FeO + CO_2 \quad \text{(R14)}$$

$$FeO + CO \rightarrow Fe + CO_2 \quad \text{(R15)}$$

The net reaction of R14 and R15 can be expressed as:

$$Fe_3O_4 + 4CO \rightarrow 3Fe + 4\,CO_2 \quad \text{(R16)}$$

As the temperature further increases, reaction R17 might happen to form Fe_3C.

$$3Fe + 2CO \rightarrow Fe_3C + CO_2 \quad \text{(R17)}$$

As reported by Cypres [10,58], above 600 °C, the presence of Fe_xO_y can promote the secondary formation of methane as follows

$$C + 2H_2 \xrightarrow{Fe_xO_y} CH_4 \quad \text{(R18)}$$

$$CO + 3H_2 \xrightarrow{Fe_xO_y} CH_4 + H_2O \quad \text{(R19)}$$

These analyses are in accordance with our previous kinetic analysis that the addition of $FeCO_3$ can decrease the activation energy of raw coal.

Based on the above analysis, it is essential to establish an integrated catalytic pyrolysis mechanism of the PRB coal with and without the use of Na–Fe composite catalysts to present a theoretical framework for understanding the experiment, as shown in Fig. 13.

Conclusions

Four model-free methods were applied to study the pyrolysis kinetics of a Powder River Basin coal with a Na–Fe composite catalyst. The results show that the nonlinear VA method appears to have the most reasonable E values in the range of α considered. Further, the A_n (random-nucleation and nuclei growth model) appears to be the appropriate reaction model for the raw coal pyrolysis with and without the use of Na_2CO_3–$FeCO_3$ composite catalyst. As an effective catalyst for coal gasification, Na_2CO_3 improves the activation energy of raw coal pyrolysis. The composite Na–Fe not only adjusts the product selectivity, but also decreases the activation energy of raw coal pyrolysis with only the addition of Na_2CO_3. It is expected that these findings will help the development of catalytic coal pyrolysis from both the scientific and technological aspects.

Acknowledgements

The authors gratefully acknowledge the Department of Energy (DE-FE0023999) and the Idaho National Laboratory Directed Research and Development Program under DOE

Idaho Operations Office Contract DE-AC07-05ID14517 for supporting this work.

Appendix A. Supplementary data

Supplementary data related to this article can be found at https://doi.org/10.1016/j.ijhydene.2018.02.102.

REFERENCES

[1] Schobert HH, Song C. Chemicals and materials from coal in the 21st century. Fuel 2002;81:15–32.
[2] Miura K. Mild conversion of coal for producing valuable chemicals. Fuel Process Technol 2000;62:119–35.
[3] Liu Q, Hu H, Zhou Q, Zhu S, Chen G. Effect of inorganic matter on reactivity and kinetics of coal pyrolysis. Fuel 2004;83:713–8.
[4] Altuntas Öztas N, Yürüm Y. Effect of catalysts on the pyrolysis of Turkish Zonguldak bituminous coal. Energy Fuel 2000;14:820–7.
[5] Li C-Z, Sathe C, Kershaw JR, Pang Y. Fates and roles of alkali and alkaline earth metals during the pyrolysis of a Victorian brown coal. Fuel 2000;79:427–38.
[6] Chen H, Li B, Zhang B. Effects of mineral matter on products and sulfur distributions in hydropyrolysis. Fuel 1999;78:713–9.
[7] Imran A, Bramer EA, Seshan K, Brem G. High quality bio-oil from catalytic flash pyrolysis of lignocellulosic biomass over alumina-supported sodium carbonate. Fuel Process Technol 2014;127:72–9.
[8] Shie J-L, Lin JP, Chang CY, Lee DJ, Wu CH. Pyrolysis of oil sludge with additives of sodium and potassium compounds. Resour Conserv Recy 2003;39:51–64.
[9] Popa T, Fan M, Argyle MD, Dyar MD, Gao Y, Tang J, et al. H_2 and CO_x generation from coal gasification catalyzed by a cost-effective iron catalyst. Appl Catal A Gen 2013;464:207–17.
[10] Cyprès R, Soudan-Moinet C. Pyrolysis of coal and iron oxides mixtures. 2. Reduction of iron oxides. Fuel 1981;60:33–9.
[11] Xu W-C, Tomita A. Effect of metal oxides on the secondary reactions of volatiles from coal. Fuel 1989;68:673–6.
[12] Lu K-M, Lee WJ, Chen WH, Lin TC. Thermogravimetric analysis and kinetics of co-pyrolysis of raw/torrefied wood and coal blends. Appl Energy 2013;105:57–65.
[13] Chen C, Ma X, He Y. Co-pyrolysis characteristics of microalgae Chlorella vulgaris and coal through TGA. Bioresour Technol 2012;117:264–73.
[14] Friedman HL. Kinetics of thermal degradation of char-forming plastics from thermogravimetry. Application to a phenolic plastic. in J Polym Sci Part C: polymer Symposia. Wiley Online Library; 1964.
[15] Flynn J, Wall L. Thermal analysis of polymer by thermogravimetric analysis. J Res Natl Bur Stand Sect A 1966;70:487.
[16] Ozawa T. A new method of analyzing thermogravimetric data. Bull Chem Soc Jpn 1965;38:1881–6.
[17] Kissinger HE. Reaction kinetics in differential thermal analysis. Anal Chem 1957;29:1702–6.
[18] Akahira T, Sunose T. Joint convention of four electrical institutes. Res Rep Chiba Inst Technol 1971;16:22–31.
[19] Vyazovkin S, Dollimore D. Linear and nonlinear procedures in isoconversional computations of the activation energy of nonisothermal reactions in solids. J Chem Inf Comput Sci 1996;36:42–5.
[20] Vyazovkin S. A unified approach to kinetic processing of nonisothermal data. Int J Chem Kinet 1996;28:95–101.
[21] Criado J, Malek J, Ortega A. Applicability of the master plots in kinetic analysis of non-isothermal data. Thermochim Acta 1989;147:377–85.
[22] Málek J. The kinetic analysis of non-isothermal data. Thermochim Acta 1992;200:257–69.
[23] Gotor FJ, Criado JM, Malek J, Koga N. Kinetic analysis of solid-state reactions: the universality of master plots for analyzing isothermal and nonisothermal experiments. J Phys Chem A 2000;104:10777–82.
[24] Popa T, Fan M, Argyle MD, Slimane RB, Bell DA, F Towler B. Catalytic gasification of a powder river basin coal. Fuel 2013;103:161–70.
[25] Monterroso R, Fan M, Argyle MD, Varga K, Dyar D, Tang JK, et al. Characterization of the mechanism of gasification of a powder river basin coal with a composite catalyst for producing desired syngases and liquids. Appl Catal A Gen 2014;475:116–26.
[26] Xu B, Lu WY, Sun Z, He T, Goroncy A, Zhang YL, Fan M. High-quality oil and gas from pyrolysis of powder river basin coal catalyzed by an environmentally-friendly, inexpensive composite iron-sodium catalysts. Fuel Process Technol 2017;167:334–44.
[27] Brown M, Dollimore D, Galwey A. In: Bamford CH, Tipper CFH, editors. Reactions in the solid state, vol. 22 of Comprehensive chemical kinetics. Amsterdam: Elsevier; 1980.
[28] Flynn JH. The 'temperature integral'—its use and abuse. Thermochim Acta 1997;300:83–92.
[29] Yan L, He B, Hao T, Pei X, Li X, Wang C, et al. Thermogravimetric study on the pressurized hydropyrolysis kinetics of a lignite coal. Int J Hydrogy Energy 2014;39:7826–33.
[30] Silvarrey LD, Phan A. Kinetic study of municipal plastic waste. Int J Hydrogy Energy 2016;41:16352–64.
[31] Ahmed I, Gupta A. Hydrogen production from polystyrene pyrolysis and gasification: characteristics and kinetics. Int J Hydrogy Energy 2009;34:6253–64.
[32] Maurya R, Ghosh T, Saravaia H, Paliwa C, Ghosh A, Mishra S. Non-isothermal pyrolysis of de-oiled microalgal biomass: kinetics and evolved gas analysis. Bioresour Technol 2016;221:251–61.
[33] Kandelbauer A, Wuzella G, Mahendran A, Taudes I, Widsten P. Model-free kinetic analysis of melamine–formaldehyde resin cure. Chem Eng J 2009;152:556–65.
[34] Flynn J. The isoconversional method for determination of energy of activation at constant heating rates: corrections for the Doyle approximation. J Therm Anal Calorim 1983;27:95–102.
[35] Burnham AK, Dinh L. A comparison of isoconversional and model-fitting approaches to kinetic parameter estimation and application predictions. J Therm Anal Calorim 2007;89:479–90.
[36] Bai F, Guo W, Lü X, Liu Y, Guo M, Li Q, Sun Y. Kinetic study on the pyrolysis behavior of Huadian oil shale via non-isothermal thermogravimetric data. Fuel 2015;146:111–8.
[37] Vyazovkin S. Modification of the integral isoconversional method to account for variation in the activation energy. J Comput Chem 2001;22:178–83.
[38] Janković B, Adnađević B, Mentus S. The kinetic study of temperature-programmed reduction of nickel oxide in hydrogen atmosphere. Chem Eng Sci 2008;63:567–75.
[39] Li Z-K, Wei XY, Yan HL, Zong ZM. Insight into the structural features of Zhaotong lignite using multiple techniques. Fuel 2015;153:176–82.
[40] Solum MS, Pugmire RJ, Grant DM. Carbon-13 solid-state NMR of Argonne-premium coals. Energy Fuel 1989;3(2):187–93.

[41] Song H, Liu G, Wu J. Pyrolysis characteristics and kinetics of low rank coals by distributed activation energy model. Energy Convers Manag 2016;126:1037–46.
[42] Casal M, Díez MA, Alvarez R, Barriocanal C. Primary tar of different coking coal ranks. Int J Coal Geol 2008;76:237–42.
[43] Tyler RJ. Flash pyrolysis of coals. 1. Devolatilization of a Victorian brown coal in a small fluidized-bed reactor. Fuel 1979;58:680–6.
[44] Hatcher PG. Chemical structural models for coalified wood (vitrinite) in low rank coal. Org Geochem 1990;16:959–68.
[45] Wen J-L, Sun SL, Yuan TQ, Xu F, Sun RC. Understanding the chemical and structural transformations of lignin macromolecule during torrefaction. Appl Energy 2014;121:1–9.
[46] Takagi H, Maruyama K, Yoshizawa N, Yamada Y, Sato Y. XRD analysis of carbon stacking structure in coal during heat treatment. Fuel 2004;83:2427–33.
[47] Sonibare OO, Haeger T, Foley SF. Structural characterization of Nigerian coals by X-ray diffraction, Raman and FTIR spectroscopy. Energy 2010;35:5347–53.
[48] Janković B. Kinetic analysis of the nonisothermal decomposition of potassium metabisulfite using the model-fitting and isoconversional (model-free) methods. Chem Eng J 2008;139:128–35.
[49] Cai J, Chen S. A new iterative linear integral isoconversional method for the determination of the activation energy varying with the conversion degree. J Comput Chem 2009;30:1986–91.
[50] Attar A. Bubble nucleation in viscous material due to gas formation by a chemical reaction: application to coal pyrolysis. AIChE J 1978;24:106–15.
[51] Hashimoto K, Miura K, Xu JJ, Watanabe A, Masukami H. Relation between the gasification rate of carbons supporting alkali metal salts and the amount of oxygen trapped by the metal. Fuel 1986;65:489–94.
[52] Solomon P, Fletcher T, Pugmire R. Progress in coal pyrolysis. Fuel 1993;72:587–97.
[53] Liu J, Jiang X, Shen J, Zhang H. Pyrolysis of superfine pulverized coal. Part 2. Mechanisms of carbon monoxide formation. Energ Convers Manage 2014;87:1039–49.
[54] Solomon PR, Hamblen DG, Carangelo RM, Serio MA, Deshpande GV. General model of coal devolatilization. Energy Fuel 1988;2:405–22.
[55] Hodek W, Kirschstein J, van Heek K-H. Reactions of oxygen containing structures in coal pyrolysis. Fuel 1991;70:424–8.
[56] Liu H, Deng Z, Jiang LX, Xu LF, Yan YH. Effect of sodiumcarboxylate on pyrolysis of Zhundong Coal. J Chem Ind Eng (China) 2016;67:4795–801.
[57] Sathe C, Pang Y, Li C-Z. Effects of heating rate and ion-exchangeable cations on the pyrolysis yields from a Victorian brown coal. Energy Fuel 1999;13:748–55.
[58] Cypres R, Soudan-Moinet C. Pyrolysis of coal and iron oxides mixtures. 1. Influence of iron oxides on the pyrolysis of coal. Fuel 1980;59:48–54.